Starting the winter season: predicting endodormancy induction through multi-process modeling

Guillaume Charrier

▶ To cite this version:

Guillaume Charrier. Starting the winter season: predicting endodormancy induction through multi-process modeling. 2021. hal-03065757v2

HAL Id: hal-03065757

https://hal.inrae.fr/hal-03065757v2

Preprint submitted on 31 Mar 2021 (v2), last revised 24 Nov 2021 (v3)

Starting the winter season: predicting endodormancy induction in walnut trees through multi-process modeling.

Running title: Predicting endodormancy induction in walnut trees

Guillaume Charrier[1]

[1]Université Clermont Auvergne, INRAE, PIAF, 63000 Clermont-Ferrand, France

*: corresponding author

Email: guillaume.charrier@inrae.fr

Tel: +33 4 43 76 14 21

UMR PIAF, INRAE Site de Crouel

5, chemin de Beaulieu

63000 Clermont-Ferrand

Abstract

Background and Aims

In perennial plants, the annual phenological cycle is sub-divided into successive stages whose completion will lead directly to the onset of the following event. A critical point is the transition between the apparent vegetative growth and the cryptic dormancy. To date, the initial date for chilling accumulation (D_{CA}) is arbitrarily set using various rules such as fixed or dynamic dates depending on environmental variables. These rules led to tremendous variability across studies and sites (from late summer until late autumn).

Methods

To test the relevancy of different D_{CA}, a dataset combining 34 dormancy release dates and 77 budburst dates in independent locations and/or years and 111 frost hardiness measurements in various orchards across France and Spain for the walnut *Juglans regia* L. cv Franquette.

Key Results

Many of the tested D_{CA} provided accurate results for the calibration and validation datasets (RMSEP < 10 and 8 days for endodormancy release and budburst dates, respectively). However, for frost hardiness, only the D_{CA} provided by the DORMPHOT model provided accurate results (RMSEP < 3°C). The best D_{CA} was thus selected using a composite index for all three processes.

Testing the prediction under current and future climatic scenario showed that in, up to 25% of French territory under RCP 8.5 scenario, ecodormancy stage is likely to be delayed although temperature is increasing. Overall, less average frost damages are expected although decennial risk (*i.e.* return period of ten years) is likely to increase in autumn in 15% of French territory.

Conclusions

In southern part of France, delayed dormancy induction and release would induce delayed budburst and blooming altering flower and fruit production, whereas North East and Massif Central parts of France may suffer higher frost risks from late frost acclimation. Finally, this study describes relationships between climatic variables and plant phenological processes to build metamodels predicting next century's phenological cycles at the global scale.

Introduction

In frost-exposed environments, deciduous trees have to timely adjust their biology and increase frost resistance by anticipating unfavorable conditions before the winter period. As observed for most stresses, avoidance and tolerance are two complementary processes driving frost resistance (Charrier *et al.*, 2011). The protection of shoot apical meristems under bud scales can be considered as an avoidance strategy. This is achieved through physiological changes allowing the transition from an apparently active (*e.g.* primary and secondary growth, leaf expansion, fruit maturation) towards a 'dormant' period. In temperate species, dormancy is a two-stage period with respect to the inhibiting factor. During endodormancy (formerly called dormancy), growth is inhibited by intrinsic factors to the bud ('endo') whereas during ecodormancy (formerly called quiescence), growth is limited by environmental factors ('eco'; Lang *et al.*, 1987). During this transition, different phenologically-related processes that are either visible (*e.g.* growth cessation, leaf fall, lignification or budset) or invisible (*e.g.* dormancy induction and release) take place. In parallel, trees transiently increase their frost tolerance through frost acclimation / deacclimation process (Charrier *et al.*, 2011).

In autumn, endodormancy release and frost acclimation are induced by the same environmental factors, namely decreasing temperature and photoperiod (Welling *et al.*, 2002; Arora *et al.*, 2003; Maurya & Bahlerao, 2017). After endodormancy was released, ecodormancy and frost deacclimation also occurs in parallel, under the control of warm temperature, in most species, eventually modulated by photoperiod in photosensitive species, such as late successional species (Basler & Körner, 2012). Process-based models using these variables as input have been developed to simulate the dormancy release and budburst dates (Chuine *et al.*, 2016), as well as frost hardiness (*e.g.* Leinonen 1996; Ferguson *et al.*, 2011; Charrier *et al.*, 2018).

Under the context of global change, it is particularly critical to accurately predict future trends in warmer climates. Since the first empirical model describing the relation between temperature and plant development, through the thermal-time concept (Réaumur, 1735), budburst and blooming models were only computing accumulation of growth-effective temperature (*i.e.* growth degree days GDD). As the starting point was set at the coldest period of the year (*i.e.* January 1st or July 1st in northern and southern hemisphere, respectively), these models provided accurate results. However, this type of model was not efficient under warmer winter areas, where temperate crop species were attempted to grow (*e.g.* Northern Africa, Middle East or South America; Balandier *et al.*, 1993). In this context, temperate perennial crops did exhibit lack of chilling and insufficient endodormancy release (Weinberger, 1950). The process of endodormancy, and related chilling accumulation, had thus been introduced into models (Weinberger, 1956; Vegis 1964). In the recent decades, naturally growing trees have also been affected by a reduction in chilling exposure throughout winter, enhancing the interest into the endodormancy stage (Gauzere *et al.*, 2019).

Two-step models, simulating endo- and ecodormancy stages, are now commonly used to predict budburst dates (Chuine *et al.*, 2016). Frost acclimation models use similar formalism with direct linkage between frost acclimation and exposure to chilling temperatures followed by frost deacclimation and exposure to forcing temperatures, respectively. In perennial plants, the completion of a stage is concomitant with the onset of the following one (Hänninen & Tanino, 2011). However, the initial date for chilling accumulation (D_{CA}) is usually arbitrarily set with various rules leading to tremendous variability across studies (from late summer until late autumn). Four different concepts of D_{CA} have been used (see Tab. S1):

- Fixed date across years and locations: from September 1st (Chuine *et al.*, 2016) until November 1st (Weinberger, 1967), for northern hemisphere,

1 - Dynamic date through a simple climatic threshold: critical temperature (*e.g.* date of the first

2 frost; Landsberg, 1974) or photoperiod (Welling *et al.*, 1997),

3 - Dynamic date through a mathematic function using a single variable such as the date of

4 minimum chilling units computed by the Utah model (Richardson *et al.*, 1974),

5 - Dynamic date through a mathematic function using interacting variables (temperature and

6 photoperiod) simulating leaf fall date (Delpierre *et al.*, 2009) or dormancy induction

7 (DORMPHOT; Caffarra *et al.*, 2011a).

8 These different approaches have mainly been used for phenological cycle prediction. Thanks

9 to a large dataset combining data from 50 years in various orchards across France and Spain for

10 *J. regia* cv Franquette, different formalism were tested to compute the effects of the onset of

11 chilling accumulation D_{CA} on the accuracy of three related processes (endodormancy,

12 ecodormancy and frost acclimation/deacclimation). The optimal model was subsequently

13 assessed for future climate prediction over France following three contrasted *scenarii*.

Material and methods

15 *Endodormancy release and budburst dates*

16 Endodormancy release dates were measured using the one-node-cutting 'forcing' test of

17 Rageau (1982). Samplings were performed every three weeks from October until May and 48

18 one-node cuttings prepared per sampling date. Buds were isolated from other parts of plant to

19 prevent correlative inhibitions (Dennis, 2003). At each sampling date, one-year-old stems were

20 sampled from five individual trees and cut in 7-cm long pieces, bearing only one node at the

21 top or less than 1 cm below the top end, for terminal and axillary buds, respectively. For axillary

22 buds, the top of the cutting was covered by paraffin wax to prevent desiccation. The bases of

23 the cuttings were immersed into tap water, weekly changed. Forty-eight cuttings were exposed

24 to optimal conditions for growth resumption (*i.e.* 16/8 hours Day/Night and 25°C constant) and

1 individually observed every 3 days. Mean time until budburst (stage 09 BBCH; Meier, 2001)

2 were computed from individual time until budburst for each cutting. After endodormancy

3 release, buds of *J. regia* cv Franquette break out after 20 days under optimal conditions

4 (Mauget, 1980; Charrier *et al.*, 2011). Endodormancy release dates were thus obtained by linear

5 interpolation between the two dates giving a time to budburst higher (or equal to) and lower (or

6 equal to) than 20 days, respectively. Budburst in the field was monitored every two to three

7 days at the different sites on five individual trees until 50% of buds reached the stage 09 of the

8 BBCH scale. The different locations and number of yearly observation are indicated in Table

9 1.

10 *Frost hardiness*

11 Frost hardiness was measured from September until budburst on five one-year-old branches

12 from different individual trees in different orchards (Tab. 1) using the electrolyte leakage

13 method (Charrier & Améglio 2011). Samples were cut into six 7-cm-long segments without

14 buds. Four of them were exposed for one hour to four different freezing temperatures among

15 this set of temperatures: -5, -10, -15, -20, -30 and -40 °C. Depending on the season, either the

16 highest or the lowest temperatures were not used. Two supplementary subsamples were

17 exposed to control (+5 °C) and maximal freezing temperature (-80 °C). Freezing and thawing

18 rates were set to 5 K h^{-1}.

19 Relative electrolytic leakage (REL) was calculated as (C1/C2) as described in Zhang &

20 Willison (1987). A sigmoidal relationship between REL and temperature (θ) was assumed for

21 each sample:

22 $$REL = \frac{a}{1+e^{b(c-\theta)}} + d \qquad (1)$$

23 where parameters a and d define asymptotes of the function, and b is the slope at the inflection

24 point c.

Frost hardiness was defined as the temperature of the inflection point (c) of the adjusted logistic sigmoid function (Repo & Lappi 1989), whereas frost sensitivity was considered to be estimated by the parameter b in percent damage per Celsius degree. The different locations and number of years and sampling dates are indicated in Table 1.

Climate data

Models were fit using observed daily mean and minimal temperature monitored by weather station, located most of the time in the same orchard and closer than 10km distance (Tab. 1). For predictive purpose, the temperature, calculated according to the CNRM-ALADIN52 model and corrected by a Q-Q method (Déqué *et al.*, 2007), were used from 8462 sites across France (Safran grid at 64km² spatial resolution; MétéoFrance). Four datasets were used as input variable: reference period (1950-2005) and three contrasted climatic *scenarii* (RCP 2.6, RCP 4.5 and RCP 8.5) for the future period (2005-2100). For each site and day, day and night length were computed depending on the latitude and day of year.

Endodormancy induction and onset of chilling accumulation

Date of the onset of chilling accumulation (D_{CA}) was computed through different functions:

i)   Fixed D_{CA} every *ca.* 10 days from DOY 182 (July 1st) until DOY 335 (November 30th).

ii) Dynamic D_{CA} based on threshold values reached by minimum temperature (T_{min}), mean temperature (T_{mean}), first frost (FF) or photoperiod.

iii) Date of minimum chilling units (CU_{min}) were computed according to the Utah model (originally developed on *Prunus persica* L. Batsch) that computes negative chilling effect for temperature higher than 16°C (Richardson *et al.*, 1974). Daily CU started were summed from DOY 182 (July 1st) until DOY 365 (December 31st) using the Utah_Model function (ChillR package; Luedeling, 2019).

iv) Predicted leaf fall dates (BBCH 97) were computed according to the thermal (LFT) and photothermal (LFPT) models developed by Delpierre *et al.* (2009) and developed in *Quercus* and *Quercus + Fagus*, respectively. Below a critical photoperiod, temperature colder than a threshold, modulated by a photoperiod function in the case of the LFPT model, are summed up to a critical value (Y_{crit}), corresponding to the leaf fall date. Both LFT and LFPT model were computed using the original or a modified set of parameters: LF(P)T_{ori} and LF(P)T_{mod}, respectively.

v) The dormancy induction state (DS) was computed according to the DORMPHOT model developed in *Betula pubescens* Ehrh. by Caffarra *et al.* (2011a). The two sigmoidal response function to low temperature and photoperiod, respectively interact through sigmoidal functions. The original (DP$_{ori}$) and two modified (DP$_E$ and DP$_L$, for early and late, respectively) sets of parameters were used.

Endodormancy release and budburst

Starting from D$_{CA}$, the sum of CU was modeled according to the inverse of the Richardson function (Richardson *et al.*, 1974) which was defined as the best function predicting endodormancy release dates in walnut trees (Chuine *et al.*, 2016; Charrier *et al.*, 2018). According to the sequential paradigm, the date where $CU(t)$ reaches the critical threshold CU$_{crit}$ (arbitrary chilling units, CU) is the date of endodormancy release (D$_{ER}$), or the transition between endodormancy and ecodormancy!

$$CU(t + 1) = CU(t) + Max\big(Min(T_{high} - \theta(t); T_{high} - T_{low}); 0\big) \qquad (2)$$

with $CU(t)$, the chilling unit at day t, T_{high}, both the temperature above which CU equals 0 and the amount of CU when temperature equals T_{low} or lower; CU being linear between T_{low} and T_{high}.

1   The ontogenetic development during ecodormancy stage was modeled according to a

2   sigmoid function (Caffarra *et al.*, 2011a). The date when *FU(t)* reaches the critical threshold

3   FU_{crit} (arbitrary forcing units, *FU*) is the budburst date (D_{BB}).

4      $$FU(t+1) = FU(t) + \frac{1}{1+e^{-slp(\theta(t)-T_{50})}} \tag{3}$$

5   with *FU(t)*, the forcing unit at day t, slp, the slope of the function at the temperature inducing

6   half of the maximal apparent growth rate T_{50}.

7   *Frost hardiness and frost damages*

8   Frost hardiness and subsequent frost damages were computed using a photothermal model

9   developed on *Pinus sylvestris* L. (Leinonen, 1996) and adapted on *Juglans regia* (Charrier *et*

10   *al.*, 2018). Shortly, hardening ability (C_R) changes in relation to the different stage of the annual

11   cycle (endodormancy induction, endodormancy release, ecodormancy and growth). During

12   endodormancy and growth stages, C_R was set to 1 and 0, respectively. During endodormancy

13   induction, C_R was either considered gradually increasing from 0 to 1 during the 30 days before

14   the onset of chilling accumulation (Fixed D_{CA}). For simple dynamic D_{CA}, C_R was set to 0 until

15   the threshold was reached (CU_{min}, FF, T_{min}, T_{mean} or Photoperiod). For models describing

16   continuous process, C_R was defined as the ratio between the related variable and its critical

17   threshold (LF, LFPT and DP models). From the interaction between hardening, temperature

18   and photoperiod, a dynamic potential state of hardiness is computed throughout the year. Daily

19   changes in actual frost hardiness (FH) tend to reduce the difference between potential state of

20   hardiness and FH with a temporal lag (see complete description of the model in the original

21   publication). Frost damages are computed on a daily basis through the relation between FH,

22   frost sensitivity (FS, slope at FH) and minimum temperature θ_{min} as:

23    $$FD = \frac{1}{1+e^{FS(FH-\theta_{min})}} \tag{4}$$

24   *Model calibration depending on the onset of chilling accumulation*

Three different sub-models, namely endodormancy release, ecodormancy release and frost hardiness, were calibrated one after the other, as they were interrelated. To minimize sums of square between observed and predicted values, the nls function was used (Gauss-Newton algorithm), with different sets of starting values at minimum, average and maximum ranges of parameter realistic values.

For endodormancy release model, one parameter was optimized (Tab. S2): CU_{crit} corresponding to the sum of chilling units to release endodormancy. The other parameters were set to the values defined by Chuine *et al.* (2016). The dataset was split into calibration and validation datasets containing 18 observations from 6 sites and 16 observations from 5 sites, respectively (Tab. 1).

For ecodormancy model, one parameter was optimized (Tab. S2): FU_{crit} corresponding to the sum of forcing units to break buds. The endodormancy model used to predict D_{ER} was the best from the previous step and the other parameters set to the values described in Charrier *et al.* (2018). The dataset was split into calibration and validation datasets containing 41 observations from 7 sites and 36 observations from 4 sites, respectively (Tab. 1).

For frost hardiness model, seven parameters were optimized (Tab. S2): T_1 (Upper limit of the efficient temperature range), T_2 (Lower limit of the efficient temperature range), NL_1 (Lower limit of the efficient nyctiperiod range), NL_2 (Upper limit of the efficient nyctiperiod range), δ (Part of FHMax under temperature control), τ (Time constant) and FU_{critR} (Amount of forcing units for hardening competence). The endodormancy and ecodormancy models used to predict D_{ER} and D_{BB}, were the best from the previous steps and the other parameters set to the values described in Charrier *et al.* (2018). The dataset was split into calibration and validation datasets containing 60 observations (6 winter periods) from 2 sites and 51 observations (5 winter periods) from 5 sites, respectively (Tab. 1).

1 The quality of the fit and the predictive ability of the models depending on D_{CA} were assessed

2 for calibration and validation datasets computing Root Mean Square Error (RMSE) and

3 Predictive Root Mean Square Error (RMSEP), respectively:

4
$$RMSE(P) = \sqrt{\frac{\sum_{i=1}^{n}(\hat{y}_i - y_i)^2}{n}} \tag{5}$$

5 with $\hat{y}_i$ the predicted values for an observation I and y_i the observed values for an observation i

6 As the different D_{CA} provided contrasted results among models, a composite performance index

7 was used, defined as :

8
$$PI = \frac{RMSE_{endoD_i}}{max(RMSE_{endoD})} + \frac{RMSE_{ecoD_i}}{max(RMSE_{ecoD})} + \frac{RMSE_{FH_i}}{max(RMSEP_{FH})} + \frac{RMSEP_{endoD_i}}{max(RMSEP_{endoD})} +$$

9
$$\frac{RMSEP_{ecoD_i}}{max(RMSEP_{ecoD})} + \frac{RMSEP_{FH_i}}{max(RMSEP_{FH})} \tag{6}$$

10 Results

11 *Effects of D_{CA} on model accuracy*

12 Fixed D_{CA} only had a relatively small effect on the quality of the fit ($12.3 < RMSE_{endoD} <$

13 15.1 days; coefficient of variation CV = 6.8% for a 153 days range) and the predictive ability

14 of D_{ER} ($8.3 < RMSEP_{endoD} < 11.8$ days; CV = 11.7%). Fixed D_{CA} between DOY 223 (Aug. 11th)

15 and 274 (Oct. 1st) are relatively efficient to simulate CU accumulation with respect to D_{ER}. The

16 effect of various D_{CA} on the prediction of D_{BB} was also relatively low for the quality of the fit

17 ($7.1 < RMSE_{ecoD} < 8.6$ day; CV = 6.1%) and the predictive ability ($6.9 < RMSEP_{ecoD} < 8.1$

18 days; CV = 4.7%). A wider range of fixed D_{CA}, *i.e.* between 223 and 325 (Nov. 21st), similarly

19 performed for D_{BB} prediction. Annual phenological cycle (D_{ER} and D_{BB}) was thus best predicted

20 when D_{CA} was set to DOY 254 (*i.e.* Sep. 11th). For frost hardiness, fixed D_{CA} earlier than DOY

21 305 (Nov. 1st) provided highly efficient fit (RMSE < 2.0°C). However, the prediction was not

22 accurate enough, as RMSEP was almost twice higher ($3.2 < RMSEP < 3.9$°C).

1   The D_{CA} returned by the various dynamic functions were highly different across France:

2   from DOY 182 ± 5 to 312 ± 14 (median $\pm$ SD; Fig. 1A). Four groups of earliness can be defined:

3   very early (T_{min} and photoperiod), early (DP_E, $LFPT_{mod}$ and LFT_{mod}), intermediate (CU_{min}) and

4   late (LFT_{ori}, $LFPT_{ori}$, DP_{ori}, DP_L and FF). All the dynamic D_{CA} computed via different functions

5   exhibited highly significant correlation with mean annual temperature of the site (Fig. 1B-D).

6   Simple temperature thresholds, such as T_{min} or T_{mean} did not provide accurate phenological

7   (RMSEP > 11.5 and 8.0 days for D_{ER} and D_{BB}, respectively) nor FH prediction (RMSEP >

8    $3.3°C$; Tab. 2). The D_{CA} calculated via a photoperiodic threshold was relatively efficient to

9   predict D_{BB} (RMSEP = 6.8 days), but not D_{ER} (RMSEP = 10.2 days) nor FH (RMSEP = $3.5°C$).

10   The D_{CA} computed using the Utah function did not provide accurate prediction for any

11   variable of interest (RMSEP = 14.1 days, 7.8 days and $3.5°C$ for D_{ER}, D_{BB} and FH,

12   respectively). The leaf fall thermal function (LFT), using either the original (LFT_{ori}) or the

13   modified sets of parameters (LFT_{mod}), was relatively efficient to predict D_{BB} (RMSEP = 7.23

14   days) but less efficient for D_{ER} and FH (RMSEP $\geq$ 9.2 and 3.2 for D_{ER} and FH, respectively).

15   The leaf fall photothermal function (LFPT) provided accurate predictions for phenological

16   dates (RMSEP $\leq$ 8.8 and 6.9 days for D_{ER} and D_{BB} respectively) but not for FH (RMSEP > 3.2

17   $°C$). The D_{CA} computed using the DORMPHOT function were the most efficient to predict D_{ER},

18   D_{BB} and FH, in the original and 'Late' versions of the function (DP_{ori}, and DP_L, respectively).

19   Finally, the performance index (PI) accounting for all the models and methods of computing

20   D_{CA} could not distinguish between DP_{ori} and DP_L (PI = 6.31).

21   Finally, the different processes exhibited contrasted thickness linkage with D_{CA}. For

22   ecodormancy, a wide range of fixed date (100 days range: Aug. 11th until Nov. 21st) and all the

23   computations using photoperiod as an input variable, provided good fit and predictive

24   accuracies ($RMSE_{EcoD}$ and $RMSE_{EndoD}$ lower than 8 and 7.6 days, respectively). Endodormancy

25   release was slightly more restrictive with the best predictions either provided by fixed calendar

1   dates (Aug. 11th until Oct. 1st) or dynamic functions integrating the interaction between

2   temperature and photoperiod (LFPT and DP). Frost hardiness was the most restrictive, with

3   excellent predictive accuracy when using D_{CA} computed by DORMPHOT model (DP_{ori} and

4   DP_L; RMSEP < 3.0°C) compared to all the other computations.

5   Although both DP_{ori} and DP_L performed almost equally for the three variables of interest

6   (D_{ER}, D_{BB} and FH), DP_L exhibited a slightly better correlation to predict the dynamic of Mean

7   Time until budburst (MTB) during the period of dormancy induction (R^2 = 0.262 and 0.282 for

8   DP_{ori} and DP_L, respectively; Fig. 2 A-C). Furthermore, as FH was slightly better predicted using

9   DP_L (RMSEP = 2.6°C), D_{CA} predicted by this function was selected to predict the current and

10   future frost risks (Fig. 3).

11   *Predictions under current and future climates for* Juglans regia *cv Franquette*

12   Using D_{CA} computed from DP_L endodormancy release dates under current climate exhibited

13   a structured geographical pattern across France. Endodormancy release dates spanned over a

14   60 days range (Fig. 3A): earlier in mountain area (Early December) and later on the

15   Mediterranean (South-East Mid-February) and southwestern coasts (Late January). Budburst

16   dates exhibited an opposite pattern over a 77 days range (Fig. 3B): from Mid-April in Southern

17   and Western parts until late June in mountainous area. Endodormancy release and budburst

18   dates were highly correlated to mean annual temperature, although through different functions

19   (exponential and cubic function for endodormancy release and budburst, respectively; Fig. 3C-

20   D).

21   The geographic structure was less obvious for frost damages, with very low predicted

22   damages during autumn (Fig. 4A) and spring (Fig. 4C), except in high mountain area. During

23   the winter period, higher frost damages are predicted in the northeastern part of France

24   (Burgundy, Alsace, Lorraine), in mountain areas and in the north of Rhone valley (Fig. 4B).

25   Average predicted damages in autumn and spring were highly correlated to the date of first (<-

4°C) and last frost event (< 0°C), respectively (Fig. 4D; F), whereas maximum winter damages were correlated to absolute annual temperature (Fig. 4E).

For *J. regia* cv Franquette, similar trends are observed under future climate predictions, with high delay in both the onset of dormancy and release for mean annual temperature higher than 5°C (Fig. 5A, B). However, the delay affecting endodormancy stage does not carry over toward budburst with earlier budburst with increasing temperature for lower mean annual temperature than 10°C (Fig. 5C). It should be noted that similar or earlier budburst is likely to happen for higher temperature, and this may be observed in up to one quarter of France at the end of the XXIst century: from 5 (RCP 4.5) to 27% (RCP8.5 scenario) of the French territory in 2051-2100 (Fig. 6). The results are geographically consistent with the use of a fixed D_{CA}, but through a wider range in 2051-2100 (Fig. S3). Although such a delay is not forecasted within the 'Noix de Grenoble' Protected Designation of Origin area (Middle East), budburst would be delayed in most of the 'Noix du Périgord' area (Middle West) under RCP8.5 scenario (75.1% 2006-2050 and 94.2% 2051-2100). Overall, frost damages are expected to decrease, on average, all over France (Fig. S1). However, in North East and Massif Central, higher decennial risks are predicted under RCP 2.6 *scenario* (2006-2051; Fig. S2).

Discussion

Defining the initial date for cyclical processes is a critical issue. To predict annual phenological cycle in perennial organisms, such as trees, various empirical rules have been used so far. The onset of chilling accumulation during endodormancy stage (D_{CA}) had, for instance, been arbitrarily set using fixed dates across years and locations (Chuine *et al.*, 2016) or, under the dependence of environmental factors controlling the induction of dormancy (Caffarra *et al.*, 2011b). In the current study, long-term observations of phenological stages (endodormancy release and budburst) and related processes (frost acclimation and deacclimation) were used in

1 various environmental conditions and showed that the DORMPHOT model was the most

2 relevant to predict winter biology in walnut trees.

3 Depending on the studied process, not all computation performed equally (Tab. 2). The

4 effect of D_{CA} on ecodormancy and budburst was buffered during endodormancy release. From

5 a budburst perspective, various rules for D_{CA} computation can thus be considered as valid,

6 although they all consider a potential effect of photoperiod, either directly or indirectly via fixed

7 date (Welling *et al.*, 1997; Chuine and Régnière, 2017). A narrower range of fixed date and

8 fewer dynamic computations of D_{CA} (DORMPHOT and LFPT models) provided accurate

9 predictions for endodormancy release dates. However, providing predictive rules only based on

10 one or two phenological stages, even though with a large number of measurements (more than

11 100 dates, combining endodormancy and budburst, in the present study) does not provide

12 sufficient details for continuous process modeling. Introducing frost hardiness as a co-variable

13 of dormancy induction and release provided higher temporal resolution into these concurring

14 processes (Welling & Palva, 2006; Charrier *et al.*, 2011; Hanninen, 2016). Through a multi

15 criterion analysis, the D_{CA} simulated by the DORMPHOT model provided the most accurate

16 predictions. This model, originally developed in *Betula pubescens*, is thus relevant for other

17 deciduous species such as *Juglans regia*. The conceptual development of this model is indeed

18 based on experimental results combining photoperiod and temperature manipulation (Caffarra

19 *et al.*, 2011b), whereas other formalisms were based on empirical observations (*e.g.* leaf fall).

20 Photoperiod and temperature are intimately related in controlling annual weather dynamics.

21 However, temperature fluctuation is much higher at a given date of the year which could induce

22 high variability in the onset of the winter season (see *e.g.* Fig.1). Since dormancy induction and

23 frost acclimation are lengthy processes (*e.g.* ca. 1-2 month), perennial plants cannot only rely

24 on temperature changes that can be too sudden for the onset of winter rest (Caffarra *et al.*,

25 2011a). Both photoperiod and temperature variables thus affect annual phenological cycle in

perennial plants, although at different ratio across species. Photoperiod is for instance predominant in *Populus* (Kalcsits *et al.*, 2009) and *Vitis* (Fennel & Hoover, 1991), while temperature in *Malus* and *Pyrus* (Heide & Prestrud, 2005) and *Sorbus* (Heide, 2011). The interaction of both photoperiod and temperature has been showed in *Prunus* (Heide, 2008). Integrating both variables is an interesting strategy to prevent dormancy induction during cold late summer (without frost risks) while maintaining physiological activity under extended warm periods. It has been hypothesized that the modulation of photoperiod sensitivity by temperature may be related by thermal effect on phytochrome perception of day length (Mølmann *et al.*, 2005).

The selected rule for D_{CA}, predicting a delayed chilling accumulation in warmer locations (> 7°C MAT; Fig. 1C; 5A) would further delay endodormancy release in such area (Fig. 3 A, C). However, cold weather would limit ontogenetic development during ecodormancy, providing a negative picture of D_{ER} vs D_{BB} (Fig. 3). Under future climatic conditions such as predicted by RCPs *scenarii*, this picture is likely to be blurred as the tipping point for budburst of *J. regia* cv Franquette would be achieved (*ca.* 14°C MAT). Below 14°C, endodormancy would be released and warmer temperature of the winter-spring period lead to earlier budburst.

Date of first frost (< 0°C), minimum temperature and date of late frost (<-4°C) appear as good proxies to predict early, maximum and late frost damages, respectively (Fig. 4D-F). Predicted minimal temperature are expected to decrease as well and, even though flushing buds would be highly vulnerable to late frost, they are likely not to be exposed to damaging temperature (Fig. 4). Although climate models agree on the average trend, they are still unclear on the climate extreme events such as early and late frost events. Notably, the decennial damages (*i.e.* maximum damage occurring every ten years) may increase in North East and Massif Central area (Fig. S2). The relative balance between photo- and thermosensitivity is likely to be a critical trait explaining this trend. In the near future in these areas, minimum

temperature are still likely to happen while dormancy induction and frost acclimation would be delayed by mean temperature increase.

Above the 14°C threshold, endodormancy induction and release would be more delayed than ecodormancy hastened, resulting in delayed budburst due to a lack of chilling, compared to the present situation. This situation would cover up to one quarter of France under RCP 8.5 scenario (Fig. 6). Although it would significantly reduce frost damages, even under false spring *scenarii*, lack of chilling would induce severe agronomic troubles such as erratic patterns of blooming, floribondity, and potential dischronism with anthesis. A similar pattern is also expected using fixed date (see Fig S3).

With respect to French nuts production, both IGP regions would face distinct threats as they stand on both sides of the 14°C MAT tipping point. In the Périgord, chilling requirements are likely not to be met and lower chilling varieties have to be selected, as the current ones do not exhibit variability for this trait (Charrier *et al.*, 2011). In Grenoble, earlier budburst dates are expected, leading to higher exposure to frost events, and varieties with higher forcing requirements may help to stabilize the production (Charrier *et al.*, 2018). However, both regions seem relatively safe with respect to frost damages.

Conclusions and perspectives

This study highlighted the relevance of dynamic dates for simulating annual phenological cycle and frost acclimation. The DORMPHOT model, integrating temperature and photoperiodic control of dormancy induction, is the most efficient for all studied processes. On one hand, higher decennial damages would be observed in the near future on *ca.* 15% of French territory because of late frost acclimation. On the other hand, the tipping point for phenological processes is likely to be reached during the XXIst century with chilling requirements that are

1   likely not to be fulfilled. The correlation between MAT, phenological stages and frost damages

2   is an important tool, to build relevant meta-models at the global scale.

3

REFERENCES

Arora, R., Rowland, L. J., & Tanino, K. (2003). Induction and release of bud dormancy in woody perennials: a science comes of age. *HortScience*, *38*(5), 911-921.

Balandier, P., Gendraud, M., Rageau, R., Bonhomme, M., Richard, J. P., & Parisot, E. (1993). Bud break delay on single node cuttings and bud capacity for nucleotide accumulation as parameters for endo-and paradormancy in peach trees in a tropical climate. *Scientia Horticulturae*, *55*(3-4), 249-261.

Basler, D., & Körner, C. (2012). Photoperiod sensitivity of bud burst in 14 temperate forest tree species. *Agricultural and Forest Meteorology*, *165*, 73-81.

Caffarra, A., Donnelly, A., Chuine, I., & Jones, M. B. (2011a). Modelling the timing of Betula pubescens budburst. I. Temperature and photoperiod: a conceptual model. *Climate Research*, *46*(2), 147-157.

Caffarra, A., Donnelly, A., & Chuine, I. (2011b). Modelling the timing of Betula pubescens budburst. II. Integrating complex effects of photoperiod into process-based models. *Climate research*, *46*(2), 159-170.

Charrier, G., & Améglio, T. (2011). The timing of leaf fall affects cold acclimation by interactions with air temperature through water and carbohydrate contents. *Environmental and Experimental Botany*, *72*(3), 351-357.

Charrier, G., Bonhomme, M., Lacointe, A., & Améglio, T. (2011). Are budburst dates, dormancy and cold acclimation in walnut trees (Juglans regia L.) under mainly genotypic or environmental control?. *International journal of biometeorology*, *55*(6), 763-774.

Charrier, G., Chuine, I., Bonhomme, M., & Améglio, T. (2018). Assessing frost damages using dynamic models in walnut trees: exposure rather than vulnerability controls frost risks. *Plant, Cell & Environment*, *41*(5), 1008-1021.

Chuine, I., & Régnière, J. (2017). Process-based models of phenology for plants and animals. *Annual Review of Ecology, Evolution, and Systematics*, *48*, 159-182.

Chuine, I., Bonhomme, M., Legave, J. M., García de Cortázar-Atauri, I., Charrier, G., Lacointe, A., & Améglio, T. (2016). Can phenological models predict tree phenology accurately in the future? The unrevealed hurdle of endodormancy break. *Global Change Biology*, *22*(10), 3444-3460.

Delpierre, N., Dufrêne, E., Soudani, K., Ulrich, E., Cecchini, S., Boé, J., & François, C. (2009). Modelling interannual and spatial variability of leaf senescence for three deciduous tree species in France. *Agricultural and Forest Meteorology*, *149*(6-7), 938-948.

Dennis, F. G. (2003). Problems in standardizing methods for evaluating the chilling requirements for the breaking of dormancy in buds of woody plants. *HortScience*, *38*(3), 347-350.

Déqué, M., Rowell, D. P., Lüthi, D., Giorgi, F., Christensen, J. H., Rockel, B., ... & van den Hurk, B. J. J. M. (2007). An intercomparison of regional climate simulations for Europe: assessing uncertainties in model projections. *Climatic Change*, *81*(1), 53-70.

Fennell, A., & Hoover, E. (1991). Photoperiod influences growth, bud dormancy, and cold acclimation in Vitis labruscana and V. riparia. *Journal of the American Society for Horticultural Science*, *116*(2), 270-273.

Ferguson, J. C., Tarara, J. M., Mills, L. J., Grove, G. G., & Keller, M. (2011). Dynamic thermal time model of cold hardiness for dormant grapevine buds. *Annals of botany*, *107*(3), 389-396.

Gauzere, J., Lucas, C., Ronce, O., Davi, H., & Chuine, I. (2019). Sensitivity analysis of tree phenology models reveals increasing sensitivity of their predictions to winter chilling temperature and photoperiod with warming climate. *Ecological Modelling*, *411*, 108805.

Hänninen, H., & Tanino, K. (2011). Tree seasonality in a warming climate. *Trends in plant science*, *16*(8), 412-416.

Hänninen, H. (2016). Boreal and temperate trees in a changing climate. *Dordrecht: Springer. doi*, *10*, 978-94.

Heide, O. M., & Prestrud, A. K. (2005). Low temperature, but not photoperiod, controls growth cessation and dormancy induction and release in apple and pear. *Tree physiology*, *25*(1), 109-114.

Heide, O. M. (2008). Interaction of photoperiod and temperature in the control of growth and dormancy of Prunus species. *Scientia Horticulturae*, *115*(3), 309-314.

Heide, O. M. (2011). Temperature rather than photoperiod controls growth cessation and dormancy in Sorbus species. *Journal of experimental botany*, *62*(15), 5397-5404.

Kalcsits, L. A., Silim, S., & Tanino, K. (2009). Warm temperature accelerates short photoperiod-induced growth cessation and dormancy induction in hybrid poplar (Populus× spp.). *Trees*, *23*(5), 971-979.

Landsberg, J. J. (1974). Apple fruit bud development and growth; analysis and an empirical model. *Annals of Botany*, *38*(5), 1013-1023.

Lang, G. A., Early, J. D., Martin, G. C., & Darnell, R. L. (1987). Endo-, para-, and ecodormancy: physiological terminology and classification for dormancy research. *HortScience*, *22*(3), 371-377.

Leinonen, I. (1996). A simulation model for the annual frost hardiness and freeze damage of Scots pine. *Annals of Botany*, *78*(6), 687-693.

Luedeling, E. (2019) Statistical Methods for Phenology Analysis in Temperate Fruit Trees, chillR Package.

Mauget, J. C., (1980). Dormance et précocité de débourrement des bourgeons chez quelques cultivars de Noyer (Juglans regia L.).

Maurya, J. P., & Bhalerao, R. P. (2017). Photoperiod-and temperature-mediated control of growth cessation and dormancy in trees: a molecular perspective. *Annals of botany*, *120*(3), 351-360.

Meier, U. (2001). Growth stages of mono- and dicotyledonous plants. BBCH Monograph. doi: 10.5073/bbch0515.

Mølmann, J. A., Asante, D. K., Jensen, J. B., Krane, M. N., Ernstsen, A., Junttila, O., & Olsen, J. E. (2005). Low night temperature and inhibition of gibberellin biosynthesis override phytochrome action and induce bud set and cold acclimation, but not dormancy in PHYA overexpressors and wild-type of hybrid aspen. *Plant, Cell & Environment*, *28*(12), 1579-1588.

Rageau, R. (1982). Etude expérimentale des lois d'action de la température sur la croissance des bourgeons floraux du pêcher (*Prunus* persica L. Batsch) pendant la postdormance.

Réaumur, R. A. F. d. 1735. Observations du thermomètre, faites à Paris durant l'année 1735, comparées avec celles qui ont été faites sous la ligne, à l'isle de France, à Alger et quelques unes de nos isles de l'Amérique. Mémoires de l'Académie des Sciences de Paris.

Repo, T., & Lappi, J. (1989). Estimation of standard error of impedance-estimated frost resistance. *Scandinavian Journal of Forest Research*, *4*(1-4), 67-74.

Richardson, E. A., EA, R., SD, S., & DR, W. (1974). A model for estimating the completion of rest for" Redhaven" and" Elberta" peach trees.

Vegis, A. (1964). Dormancy in higher plants. *Annual review of plant physiology*, *15*(1), 185-224.

Weinberger, J. H. (1950). Chilling requirements of peach varieties. In *Proceedings. American Society for Horticultural Science* (Vol. 56, pp. 122-8).

Weinberger, J. H. (1956). Prolonged dormancy trouble in peaches in the southeast in relation to winter temperatures. Journal of the American Society for Horticultural Science,6 7, 107-112.

Weinberger, J. H. (1967). Some temperature relations in natural breaking of the rest of Peach flower buds in the San Joaquin Valley, California. Proceedings of the American Society for Horticultural Science, 51, 84-89.

Welling, A., & Palva, E. T. (2006). Molecular control of cold acclimation in trees. *Physiologia Plantarum*, *127*(2), 167-181.

Welling, A., Kaikuranta, P., & Rinne, P. (1997). Photoperiodic induction of dormancy and freezing tolerance in Betula pubescens. Involvement of ABA and dehydrins. *Physiologia Plantarum*, *100*(1), 119-125.

Welling, A., Moritz, T., Palva, E. T., & Junttila, O. (2002). Independent activation of cold acclimation by low temperature and short photoperiod in hybrid aspen. *Plant Physiology*, *129*(4), 1633-1641.

Zhang, M. I. N., & Willison, J. H. M. (1987). An improved conductivity method for the measurement of frost hardiness. Canadian Journal of Botany, 65, 710–715.

Acknowledgements

Figure captions

Figure 1. A Distribution of date at the onset of chilling accumulation T_0 across France over the 1950-2005 period according to different computations: T_{min} minimum temperature (lower than 15.28°C), DP DORMPHOT model from different sets of parameters (O: original, E early, L Late), LFT_{mod} Leaf Fall model (thermal version modified), LFPT Leaf Fall model Photothermal version Original and modified. B, C and D T0 depending on mean annual temperature.

Figure 2 Mean time until budbreak at 25°C (MTB) depending on the day after September 1st (A), Dormancy stage computed according to the DORMPHOT model (B original version, C, late version).

Figure 3. A-B. Average dates of endodormancy release (A) and budburst (B) predicted across France under current climatic conditions. **C-D.** Average dates of endodormancy release (C) and budburst (D) depending on mean annual temperature (°C) across France.

Figure 4. A-C. Average frost damages predicted across France under current climatic conditions in autumn (A), winter (B) and spring (C). **D.** Average early frost damages depending on the average date of the first frost lower than 0°C. **E.** Average maximum frost damages depending on the average annual minimum temperature. **F.** Average late frost damages depending on the average date of the last frost lower than -4°C.

Figure 5. A-C. Average date of onset of dormancy (A), endodormancy release (B), budburst (C) over France depending on the mean annual temperature under current climate (gray), RCP 2.6 (2006-2051 cyan, 2051-2100 blue), RCP 4.5 (2006-2051 green, 2051-2100 yellow), and RCP 8.5 *scenarii* (2006-2051 purple, 2051-2100 red). **D.** Average predicted autumn early frost damages depending on the date of first frost (<0°C) **E.** Average predicted maximum winter frost damages depending on the mean absolute minimum temperature **F.** Average predicted spring late frost damages depending on the date of last frost (<-4°C). Each dot represent the average of the considered period at 8 x 8km spatial resolution, black line represent the best non-linear regression.

Figure 6. Relative change in predicted average budburst date across France according to different climatic *scenarii* and time periods (earlier and later budburst dates than the mean are represented in blue and red, respectively).

Table 1. Site and dataset description

Location	Elevation (m asl.)	Latitude °	Longitude °	Mean annual temperature (°C)	Minimum temperature (°C)	Absolute minimum temperature (°C)	Number of freezing events	First Frost (Autumn) DOY	Last Frost (Spring) DOY	Number of observations (years and number of dates in brackets)					
										Endodormancy Release		Budburst		Frost Hardiness	
										Calibration	Validation	Calibration	Validation	Calibration	Validation
Balandran	69	43.758	4.516	16.90	12.00	-3.78	14.5	340	50	1	1	0	0	0	0
Chatte	304	45.143	5.282	13.62	8.15	-9.39	61.7	308	102	0	0	12	11	0	1 (6)
Creysse	115	44.887	1.597	14.65	8.52	-8.50	52.4	309	104	0	0	13	12	0	1 (8)
Crouël	340	45.779	3.142	13.25	9.26	-11.51	59.6	302	108	13	12	4	4	5 (49)	2 (21)
Orcival	1150	45.683	2.842	12.92	7.72	-12.13	97.4	291	126	1	1	1	0	0	0
Terrasson	90	45.136	1.300	14.61	8.96	-9.69	47.4	311	100	1	1	1	0	0	0
Theix	945	45.706	3.021	9.70	6.22	-15.11	100.3	282	129	1	1	1	0	1 (11)	1 (9)
Toulenne	22	44.557	-0.263	15.38	10.56	-6.09	25.9	325	74	1	0	9	9	0	0
Mas Bové	112	41.170	1.169	15.87	10.81	-4.05	14.9	343	47	0	0	0	0	0	1 (7)

1 **Table 2.** Quality assessment of different models. RMSE(P) less than 15% higher than minimum RMSE or RMSEP are indicated in bold. Dates for
2 onset of chilling accumulation (D$_{CA}$) were either fixed or computed according to date of first frost (FF), minimum temperature (T$_{min}$), mean
3 temperature (T$_{mean}$), photoperiod, minimum chilling unit (CU$_{min}$), Leaf fall using temperature (LFT) and temperature and photoperiod (LFPT) and
4 dormphot (DP). Ori and mod refer to the original published version (ori) or modified for walnut (mod), E and L for Early and Late.

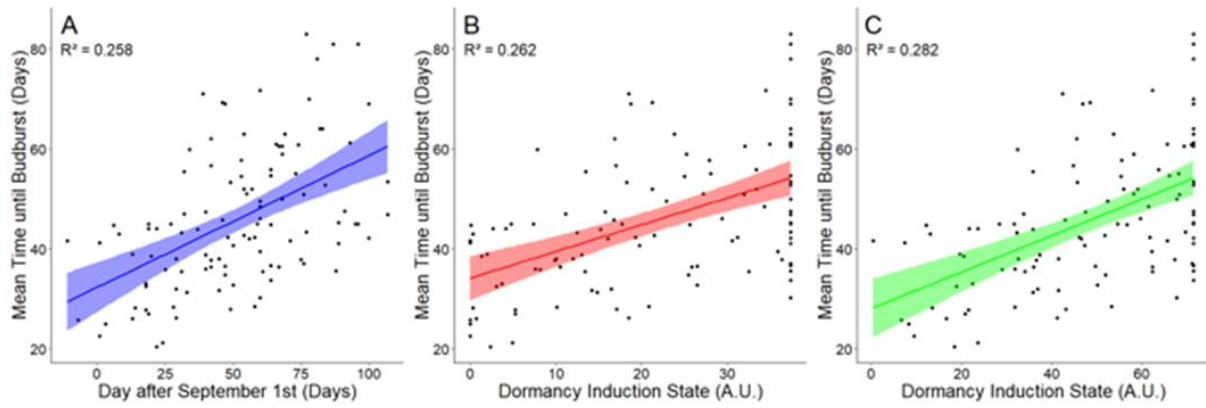| | | | Endodormancy | | Budburst | | Frost | | PI |
			Release Date		Date		Hardiness		
Type	Function	D$_{CA}$	RMSE	RMSEP	RMSE	RMSEP	RMSE	RMSEP	
			(days)	(days)	(days)	(days)	(°C)	(°C)	
Fixed		182 (Jul. 1st)	**12.84**	11.84	8.58	8.08	**1.79**	3.52	7.31
		192 (Jul. 11th)	**12.64**	11.48	8.44	**7.57**	**1.79**	3.39	7.10
		202 (Jul.21st)	**12.41**	10.73	8.25	**7.28**	**1.80**	3.42	6.94
		213 (Aug. 1st)	**12.33**	10.06	8.06	**7.14**	**1.79**	3.46	6.81
		223 (Aug. 11th)	**12.65**	**9.36**	**7.78**	**6.89**	**1.78**	3.49	6.68
		233 (Aug. 21st)	**12.68**	**8.71**	**7.61**	**6.85**	**1.78**	3.49	6.58
		244 (Sep. 1st)	**12.87**	**8.75**	**7.39**	**7.03**	**1.79**	3.48	6.59
		254 (Sep. 11th)	**13.19**	**8.49**	**7.26**	**6.88**	**1.77**	3.47	6.53
		264 (Sep. 21st)	**13.70**	**8.80**	**7.15**	**7.24**	**1.74**	3.24	6.55
		274 (Oct. 1st)	**13.80**	**8.47**	**7.25**	**7.38**	**1.73**	3.29	6.56
		284 (Oct. 11th)	13.98	**8.29**	**7.10**	**6.93**	**1.77**	3.37	6.52
		294 (Oct. 21st)	14.39	**8.47**	**7.25**	**7.15**	**1.84**	3.30	6.64
		305 (Nov. 1st)	14.48	**9.22**	**7.45**	**7.47**	**1.84**	3.21	6.78
		315 (Nov. 11th)	14.48	9.93	**7.52**	**7.56**	2.15	3.42	7.16
		325 (Nov. 21st)	14.67	10.26	**7.46**	**7.43**	2.90	3.90	7.81
		335 (Dec. 1st)	15.10	10.33	**7.58**	7.67	3.77	3.52	8.77
Dynamic	Simple	FF	17.71	14.15	9.35	15.69	**1.90**	4.92	9.84
		T$_{min}$	**12.88**	11.93	8.55	8.03	**1.79**	3.37	7.25
		T$_{mean}$	**12.93**	11.59	8.70	8.47	**1.81**	3.38	7.31
		Photoperiod	**12.31**	10.24	**7.94**	**6.85**	**1.80**	3.46	6.78
	Complex	CU$_{min}$	16.32	14.08	8.22	7.78	**1.78**	3.48	7.74
		LFT$_{ori}$	**12.91**	10.37	**8.11**	**7.23**	**1.76**	3.22	6.81
		LFT$_{mod}$	**12.57**	9.16	**8.11**	**7.23**	**1.80**	3.19	6.83
		LFPT$_{ori}$	**13.34**	**8.67**	**7.42**	**6.72**	**1.83**	3.24	6.51
		LFPT$_{mod}$	**12.66**	**8.81**	**7.43**	**6.89**	**1.78**	3.50	6.57
		DP$_{ori}$	**13.01**	**8.81**	**7.47**	**6.61**	**1.76**	**2.87**	**6.31**
		DP$_E$	**12.05**	**8.64**	**7.73**	**7.24**	**1.80**	3.95	6.77
		DP$_L$	**12.51**	9.43	**7.52**	**7.14**	**1.70**	**2.65**	**6.31**

5

Figure captions

Figure 1. A Distribution of date at the onset of chilling accumulation T_0 across France over the 1950-2005 period according to different computations: T_{min} minimum temperature (lower than 15.28°C), DP DORMPHOT model from different sets of parameters (O: original, E early, L Late), LFT_{mod} Leaf Fall model (thermal version modified), LFPT Leaf Fall model Photothermal version Original and modified. B, C and D T0 depending on mean annual temperature.
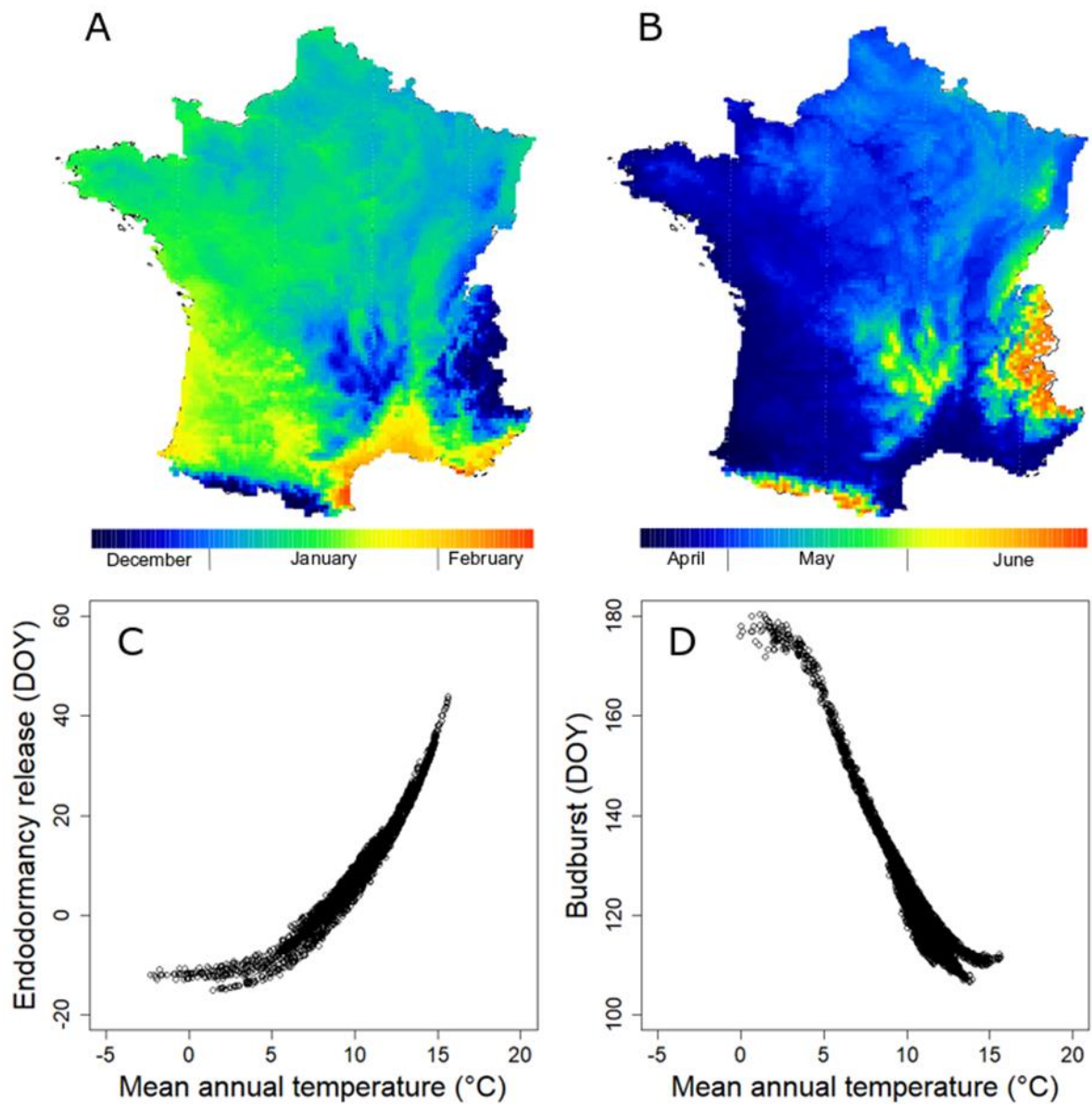
Figure 2 Mean time until budbreak at 25°C (MTB) depending on the day after September 1st (A), Dormancy stage computed according to the DORMPHOT model (B original version, C, late version).
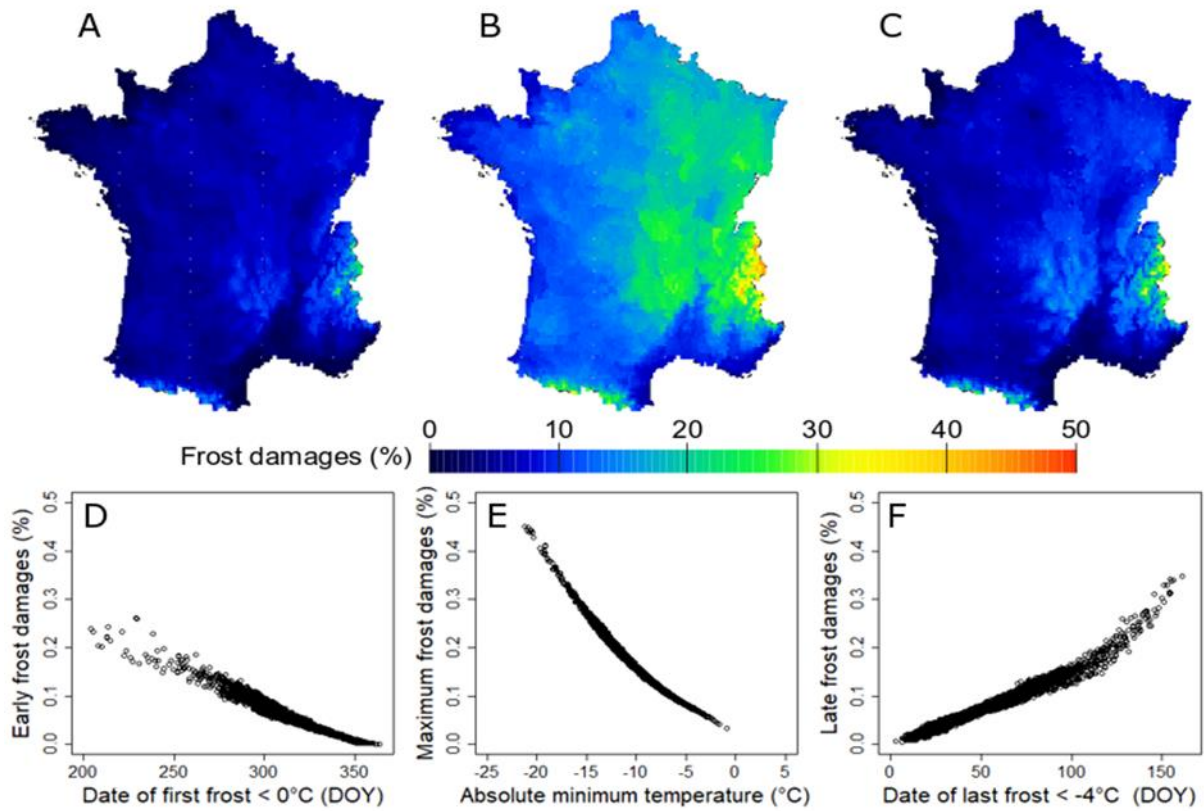
Figure 3. A-B. Average dates of endodormancy release (A) and budburst (B) predicted across France under current climatic conditions. **C-D.** Average dates of endodormancy release (C) and budburst (D) depending on mean annual temperature (°C) across France.
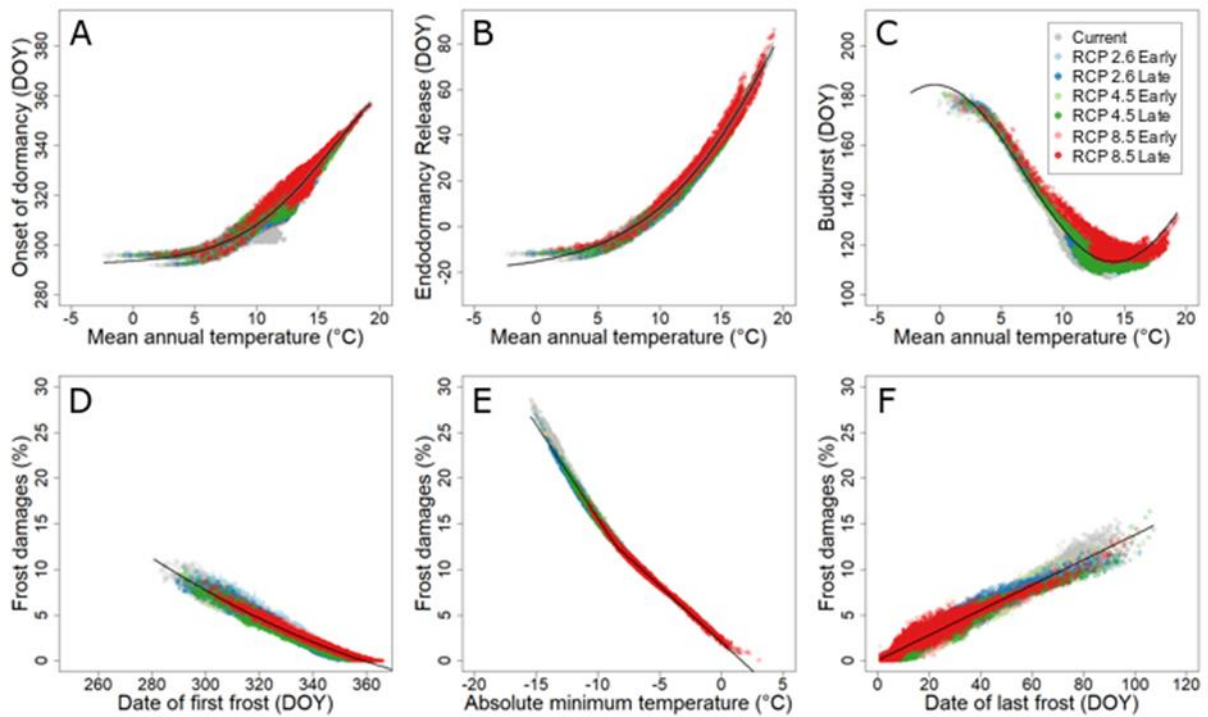
Figure 4. A-C. Average frost damages predicted across France under current climatic conditions in autumn (A), winter (B) and spring (C). **D.** Average early frost damages depending on the average date of the first frost lower than 0°C. **E.** Average maximum frost damages depending on the average annual minimum temperature. **F.** Average late frost damages depending on the average date of the last frost lower than -4°C.
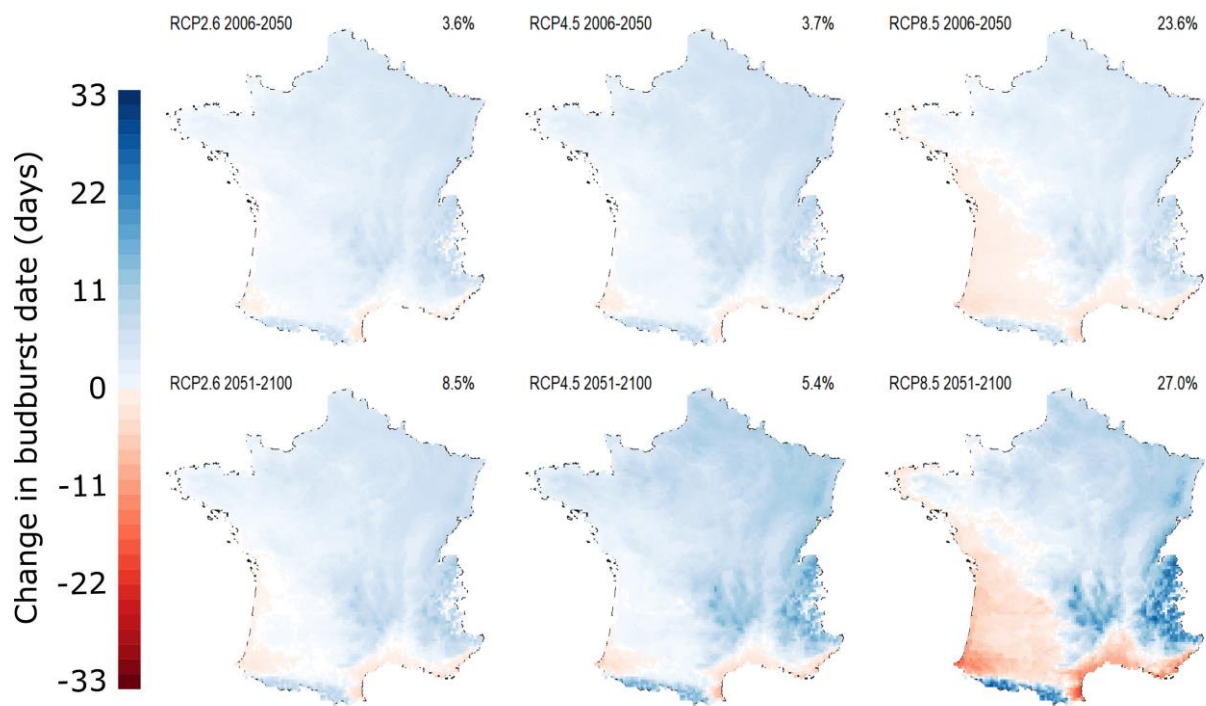
Figure 5. A-C. Average date of onset of dormancy (A), endodormancy release (B), budburst (C) over France depending on the mean annual temperature under current climate (gray), RCP 2.6 (2006-2051 cyan, 2051-2100 blue), RCP 4.5 (2006-2051 green, 2051-2100 yellow), and RCP 8.5 *scenarii* (2006-2051 purple, 2051-2100 red). **D.** Average predicted autumn early frost damages depending on the date of first frost (<0°C) **E.** Average predicted maximum winter frost damages depending on the mean absolute minimum temperature **F.** Average predicted spring late frost damages depending on the date of last frost (<-4°C). Each dot represent the average of the considered period at 8 x 8km spatial resolution, black line represent the best non-linear regression.

Figure 6. Relative change in predicted average budburst date across France
according to different climatic *scenarii* and time periods (earlier and later budburst
dates than the mean are represented in blue and red, respectively).

Supplementary material figure captions

Table S1. Examples of fixed or dynamic date of onset of chilling accumulation (DCA) across various studies aiming at modeling phenology in various species and location. Chilling models are sigmoid (Hanninen, 1990), normal (Chuine, 2000; Chuine et al., 2003), Utah (Richardson et al., 1974) and variations (smoothed Utah: Bonhomme et al., 2010, Positive Utah and positive Chill Unit for low chilling varieties: Gilreath and Buchanan, 1981), Dynamic (Fishman et al., 1987a,b), Chilling Hours (Weinberger; 1967), Bidabé (Bidabé, 1965a, b), Growing Degree Day (Ritchie and NeSmith, 1991). NH and SH mean northern and southern hemisphere, respectively.

Table S2 Optimized parameters for different DCA computations in Juglans regia cv Franquette

Figure S1. Relative change in predicted average frost damages across France according to different climatic *scenarii* (RCP 2.6, RCP 4.5, RCP 8.5), seasons (Early SON, Midwinter DJF and late risks MAM) and time periods (2006-2050 and 2051-2100). Lower and higher damages than the current mean are represented in in red and blue, respectively).

Figure S2. Relative change in predicted decennial frost damages across France according to different climatic *scenarii* (RCP 2.6, RCP 4.5, RCP 8.5), seasons (Early SON, Midwinter DJF and late risks MAM) and time periods (2006-2050 and 2051-2100). Lower and higher damages than the current 90th percentile are represented in in red and blue, respectively).

Figure S3. Relative change in predicted budburst date across France according to different climatic *scenarii* (RCP 2.6, RCP 4.5, RCP 8.5), time periods (2006-2050 and 2051-2100) and D_{CA} (September 1st vs DORMPHOT computation) Later and earlier budburst than currently are represented in in red and blue, respectively. The proportion of area showing delayed budburst is indicated for each map.